Journal of Colloid and Interface Science 340 (2009) 285–290

Contents lists available at ScienceDirect

Journal of Colloid and Interface Science

www.elsevier.com/locate/jcis

Particle electrophoresis and dielectrophoresis in curved microchannels

Junjie Zhu, Xiangchun Xuan *

Department of Mechanical Engineering, Clemson University, Clemson, SC 29634-0921, USA

ARTICLE INFO

Article history:
Received 15 July 2009
Accepted 20 August 2009
Available online 23 August 2009

Keywords:
Electrophoresis
Microchannel
Curvature
Dielectrophoresis
Focusing

ABSTRACT

Studies of particle electrophoresis have so far been limited to primarily theoretical or numerical analyses in straight microchannels. Very little work has been done on particle electrophoretic motions in real microchannels that may have one or multiple turns for reducing the devices size or achieving other functions. This article presents an experimental and numerical study of particle electrophoresis in curved microchannels. Polystyrene microparticles are found to migrate across streamlines and flow out of a spiral microchannel in a focused stream near the outer wall. This transverse focusing effect arises from the dielectrophoretic particle motion induced by the non-uniform electric field intrinsic to curved channels. The experimental observations agree quantitatively with the numerical predictions.

1. Introduction

The problem of particle electrophoresis in confined microchannels has practical significance in a variety of applications ranging from traditional gel electrophoresis [1] to electrokinetic microfluidic devices [2–4]. To date, however, studies of particle electrophoresis have been limited to primarily theoretical or numerical analyses in straight microchannels. Very little work has been done on particle electrophoretic motions in real microchannels that usually have one or multiple turns in order to fit them into the small footprint of, for example, a glass slide. It is thus important to study particle electrophoresis in curved microchannels.

Distinct from classical particle electrophoresis in an unbounded and stationary liquid [5,6], the presence of solid walls in microchannels causes at least three effects on the electrophoretic motion: (a) generating an electroosmotic flow of the suspending liquid due to the walls' nonzero charge [7]; (b) enhancing the viscous retardation of particles due to the walls' nonslip velocity [8]; and (c) altering the electric field (and thus the flow field) distribution around particles due to the walls' nonconducting condition [9]. Moreover, the last effect may induce particle dielectrophoresis as a result of polarization in nonuniform electric fields, which occurs in two circumstances [10]: when the particle moves near a wall so that the electric field around the particle is significantly distorted [11,12], and the other is when the microchannel has variable cross sections such that the applied electric field is intrinsically nonuniform [13,14].

In straight microchannels with uniform cross sections, liquid electroosmosis and particle electrophoresis remain unvaried along the flow direction. Particle dielectrophoresis is generally negligible. In the limit of thin electric double layers (as compared to the particle size, of course, even thinner as compared to the channel dimension), many theoretical and numerical studies have been conducted to determine the electrophoretic velocity of spherical or cylindrical particles moving close to a planar wall [15–17], or in a slit or cylindrical pore [18–26]. The predicted decrease in particle velocity due to the wall effects has been verified experimentally [27,28]. These retardation effects become more significant at larger double-layer thicknesses [29–31], which agrees qualitatively with a recent measurement [32]. When particles move in close proximity to a channel wall, however, the predicted wall effect is to enhance the particle electrophoretic motion [15,17,19,33,34]. This enhancement has been verified by Xuan et al. [32] in an experiment on particle electrophoresis in cylindrical capillaries.

In straight microchannels with variable cross sections, the applied electric field becomes nonuniform, causing variations in both liquid electroosmosis and particle electrophoresis. Meanwhile, particle dielectrophoresis is no longer negligible unless the particle is small (e.g., point particles [35,36]) and the imposed electric field is low. In a recent experiment on the electrophoretic motion of microparticles in a converging–diverging microchannel, Xuan et al. [37] observed that the ratio of particle velocity in the throat to that in the straight part is significantly lower than their cross-sectional area ratio. Moreover, this ratio is a strong function of both the applied electric field and the particle size. All these phenomena, as confirmed numerically by Qian's group [38,39], are the consequences of particle dielectrophoresis induced in the channel throat region. More recently, particles were observed to migrate

* Corresponding author. Fax: +1 864 656 7299.
E-mail address: xcxuan@clemson.edu (X. Xuan).

0021-9797/$ - see front matter © 2009 Elsevier Inc. All rights reserved.
doi:10.1016/j.jcis.2009.08.031

across streamlines by dielectrophoresis in microchannel constrictions formed by nonconducting posts, hurdles, or oil droplets [13,40–43]. The result is a narrower or focused particle stream downstream of the constriction. If strong DC or DC-biased AC electric fields are applied, particles may even be trapped at the entrance of the constriction [13,14,41,42,44].

In curved microchannels the applied electric field becomes nonuniform due to the variation of path length in the channel width direction; that is, the higher electric field occurs close to the inner wall of a curved channel due to the shorter path length for electric current. Therefore, both liquid electroosmosis and particle electrophoresis vary with positions within a curved microchannel, leading to increased band broadening of point like solute particles via hydrodynamic dispersion [45]. For particles with finite sizes, dielectrophoresis may take effects if the applied electric field is not too small. Davison and Sharp [46] numerically examined the electrophoretic motion of a cylindrical particle through a 90° turn. While the full hydrodynamic interactions between the particle and fluid were considered, the dielectrophoretic force induced within the turn was ignored. Dielectrophoresis was also neglected in an earlier numerical study of particle electrophoresis in a T-microchannel, where the applied electric field is nonuniform at the T-junction [47]. Such treatment may cause errors in the computed particle velocity, as discussed in Xuan and Li's recent experiment [48]. More recently, Zhu et al. [49] demonstrated sheathless electrokinetic focusing of particles along the centerline of a serpentine microchannel. They attributed this focusing to the cross-stream dielectrophoretic motion induced within the channel turns.

In this work we perform an experimental and numerical study of particle electrophoresis in spiral microchannels. This type of curved channels has been often used to reduce the device size of, for example, microreactors and micromixers [50,51]. Differently from a serpentine channel whose turns change direction alternately (i.e., left and right), a spiral channel maintains the direction of its turns. It is noticed that these two microchannels have both been recently demonstrated to focus and separate particles via inertia effects [52–57].

2. Theory

We first analyze the possible variations in speed and trajectory for particle electrophoresis through a microchannel turn of uniform width and depth, see Fig. 1. To be consistent with typical electrokinetic microfluidics where the fluid speed is on the order of mm/s [2–4,58], the inertial motions of fluid and particles are safely neglected, as the channel and particle Reynolds numbers are both very small [59,60]. Fig. 1 illustrates the electric field lines (**E**, with short arrows indicating the directions) and the contour of electric field intensity (the darker the higher) in the turn. Due to the variation in path length for electric current, electric field attains the maximum and minimum values near the inner and outer corners, respectively. Therefore, particles are subject to a transverse dielectrophoretic motion, $\mathbf{U}_{\mathrm{DEP}}$ (bold symbols denote a vector hereafter) when they move electrokinetically, $\mathbf{U}_{\mathrm{EK}}$, through the turn. In DC electric fields, particle dielectrophoresis is characterized as [61]

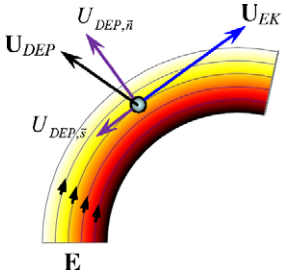

Fig. 1. Velocity analysis of particle electrophoresis in a microchannel turn of uniform width and depth. Also illustrated are the electric field lines (**E**, short arrows indicate the directions) and the contour of electric field intensity (the darker the higher).

$$\mathbf{U}_{\mathrm{DEP}} = \mu_{\mathrm{DEP}} \nabla \mathbf{E}^2 \tag{1}$$

$$\mu_{\mathrm{DEP}} = \varepsilon_{\mathrm{f}} d^2 f_{\mathrm{CM}} / 12\mu_{\mathrm{f}} \quad \text{and} \quad f_{\mathrm{CM}} = (\sigma_{\mathrm{p}} - \sigma_{\mathrm{f}})/(\sigma_{\mathrm{p}} + 2\sigma_{\mathrm{f}}), \tag{2}$$

where μ_{DEP} is the particle dielectrophoretic mobility, ε_{f} the fluid permittivity, d the particle diameter, f_{CM} the Clausius–Mossotti (CM) factor, μ_{f} the fluid viscosity, σ_{p} the particle conductivity, and σ_{f} is the fluid conductivity. Depending on the relative magnitude between σ_{p} and σ_{f}, the CM factor may be negative or positive, yielding a negative or positive dielectrophoresis [10,61]. Accordingly, $\mathbf{U}_{\mathrm{DEP}}$ may point toward the outer (for negative dielectrophoresis) or inner (for positive dielectrophoresis) corner of the turn.

Since live biological cells and polymer microparticles often behave like poor conductors in DC and low-frequency (<100 kHz) AC fields [3,62], σ_{p} is smaller than σ_{f} so that $f_{\mathrm{CM}} < 0$. Hence, these particles should be deflected across streamlines by negative dielectrophoresis and migrate toward the outer corner of the turn, as indicated in Fig. 1. It is important to note that the electric field lines illustrated in Fig. 1 are identical to the streamlines, due to the similarity between the flow and electric fields in pure electrokinetic flows [63]. Hence, we may conveniently express the particle velocity, $\mathbf{U}_{\mathrm{P}}$, in terms of streamline coordinates,

$$\begin{aligned}\mathbf{U}_{\mathrm{p}} &= \mathbf{U}_{\mathrm{EK}} + \mathbf{U}_{\mathrm{DEP}} = \mu_{\mathrm{EK}}\mathbf{E} + \mu_{\mathrm{DEP}}\nabla\mathbf{E}^2 = (U_{\mathrm{EK}} + U_{\mathrm{DEP},\vec{s}})\hat{\mathbf{s}} + U_{\mathrm{DEP},\vec{n}}\hat{\mathbf{n}} \\ &= \left(\mu_{\mathrm{EK}}E + \mu_{\mathrm{DEP}}E\frac{\partial E}{\partial s}\right)\hat{\mathbf{s}} + \mu_{\mathrm{DEP}}\frac{E^2}{\Re}\hat{\mathbf{n}},\end{aligned} \tag{3}$$

where μ_{EK} is the particle electrokinetic mobility (a combination of liquid electroosmosis and particle electrophoresis [7]), U_{EK} the streamwise electrokinetic velocity, $U_{\mathrm{DEP},\vec{s}}$ the particle dielectrophoretic velocity in the streamline direction with the unit vector $\hat{\mathbf{s}}$, $U_{\mathrm{DEP},\vec{n}}$ the dielectrophoretic particle velocity normal to the streamline direction with the unit vector $\hat{\mathbf{n}}$, E the electric field intensity, and $\Re$ is the radius of curvature of the streamline which should follow closely the radius of channel curvature in low-Reynolds-number flows.

Eq. (3) indicates that a microchannel turn causes two effects on particle electrophoresis via the curvature-induced electric field gradients (see Fig. 1): (a) the cross-stream dielectrophoretic motion, $U_{\mathrm{DEP},\vec{n}}$, shifts particles across streamlines toward the outer (if negative dielectrophoresis) or inner (if positive dielectrophoresis) corner, leading to variations in particle trajectory and speed; and (b) the streamwise dielectrophoretic motion, $U_{\mathrm{DEP},\vec{s}}$, also perturbs the particle electrokinetic velocity, though to a much smaller extent if the width and depth of the turn remain unvaried. It is the ratio of particle velocity normal and parallel to the streamline that determines the particle deflection obtained through a channel turn,

$$\frac{U_{\mathrm{DEP},\vec{n}}}{U_{\mathrm{EK}} + U_{\mathrm{DEP},\vec{s}}} = \left(\frac{\mu_{\mathrm{DEP}}}{\mu_{\mathrm{EK}} + \mu_{\mathrm{DEP}}\partial E/\partial s}\right)\frac{E}{\Re}. \tag{4}$$

Therefore, a larger electric field and/or a smaller turn radius should provide a more apparent demonstration of the above-mentioned curvature effects on particle electrophoresis. Moreover, as μ_{DEP} is proportional to the particle diameter squared [see Eq. (2)] while μ_{EK} is only a weak function of particle size [64], the velocity ratio in Eq. (4) should also increase with the rise of particle size.

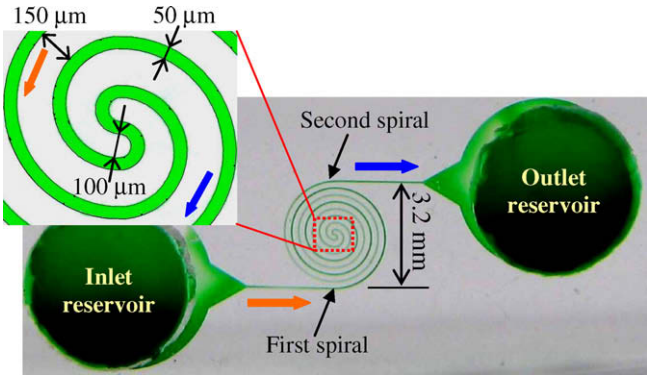

Fig. 2. Picture of the double-spiral microchannel used in the experiment with dimensions indicated in the inset. The block arrows indicate the particle flow directions in experiments, of which the inflow from the inlet reservoir takes place in the first spiral and the outflow to the outlet reservoir happens in the second spiral.

3. Experiment

Fig. 2 displays a picture of the spiral microchannel (filled with green[1] food dye for clarity) used in the experiment. It was fabricated in polydimethylsiloxane (PDMS) using the standard soft lithography technique [65]. The detailed procedure was given elsewhere [42]. The microchannel consists of two spirals that are symmetric with respect to the channel center (i.e., the junction of the two spirals) in opposite directions: the counterclockwise one is indicated as the first spiral, through which particles entered from the inlet reservoir in experiments; the clockwise one is indicated as the second spiral, through which particles exited to the outlet reservoir in experiments. Each spiral has four equally separated loops and measures 2.5 cm long in total, including the straight part from/to the reservoir. The diameter of the inner most semi-circle is 100 μm, as indicated in the inset of Fig. 2. The channel is everywhere 50 μm wide and 25 μm deep. The radial distance (or the shortest distance) between adjacent loops is 150 μm (or the center-to-center distance between loops is 200 μm).

Polystyrene particles of 5 and 10 μm in diameter (Sigma–Aldrich, USA) were re-suspended in 1 mM phosphate buffer at a concentration of at least 10^7 particles per milliliter. A 0.5% Tween 20 (Sigma–Aldrich, USA) was added to the particle solution to suppress particle adhesions to the channel. The calculated electric conductivities of the two particles are 8 and 4 μS/cm, respectively, if the surface conductance is assumed to be 1 nS [62]. As the measured electric conductivity of the buffer solution is 207 μS/cm, the CM factor, i.e., f_{CM} in Eq. (2), was determined as −0.47 and −0.49 for 5 and 10 μm particles, respectively. Electric field was supplied by a DC power supply (Glassman High Voltage Inc., High Bridge, NJ). Electrophoretic motion of particles through the spiral microchannel was visualized through an inverted microscope imaging system (TE2000-U with DS Qi1MC CCD camera, Nikon Instruments, TX), and recorded in the form of both images and live videos (about 19 frames per second).

4. Modeling

We developed a numerical model to understand and predict the observed particle electrophoretic motions in the spiral microchannel. This model is a simplified version of the one developed by Kang et al. [41,66] and has recently been applied by the authors to simulate the dielectrophoretic focusing of particles in structured microchannels [42,49]. Briefly, the perturbations of the flow and electric fields by particles were neglected in the model; so were the particle–wall and particle–particle interactions [67,68]. A correction factor, c, was introduced to account for the effects of particle size (and other effects if any) on the dielectrophoretic velocity. This is because Eq. (2) is valid only when the particle size is much smaller than the characteristic length scale of the electric field [61]. Hence, the particle velocity in Eq. (3) is rewritten as

$$\mathbf{U}_p = \mu_{EK}\mathbf{E} + c\mu_{DEP}\nabla\mathbf{E}^2. \tag{5}$$

The new velocity was then used in a particle tracing function in COMSOL (Burlington, MA) to compute the particle trajectory.

For simulation, the electrokinetic mobility, μ_{EK}, was determined by measuring the particle velocity in a straight uniform microchannel of the same width and depth as the spiral channel. We obtained an almost equal value of $\mu_{EK} = 3.2(\pm 0.3) \times 10^{-8}$ m^2/(V s) for the 5 and 10 μm particles used in experiments. The dielectrophoretic mobility, μ_{DEP}, was calculated from Eq. (2) with the typical viscosity, $\mu = 0.9 \times 10^{-3}$ kg/(m s) and permittivity $\varepsilon_f = 6.9 \times 0^{-10}$ C/(v m) for pure water at 25 °C. The values for the CM factor, f_{CM}, involved in μ_{DEP} were assigned as −0.47 and −0.49 for the 5 and 10 μm particles, as noted above. The electric field $\mathbf{E} = -\nabla\phi$ was computed by solving the 2D Laplace equation $\nabla^2\phi = 0$ using the electrostatics module in COMSOL. The boundary conditions include the voltage drop between the channel ends and the insulating condition on the channel walls. The correction factor c in Eq. (5), has recently been found to be dependent on particle size and channel geometry but insensitive to electric field [41,49,66]. Since only one channel was used in the experiment, c was determined by fitting the predicted particle trajectory to the experimental data at the electric field of 200 V/cm. The obtained c value for each particle size was then used for all other electric fields if applicable.

5. Results and discussion

Fig. 3 illustrates and compares the experimentally observed electrophoretic motions (top row: snapshot images; middle row: superimposed images) and the numerically predicted trajectories (bottom row) of 5 μm particles in the spiral microchannel. The applied DC electric field was 200 V/cm on average, corresponding to a 1000-V voltage drop across the 5-cm-long channel. The correction factor c in Eq. (5) was set to 0.6 in the modeling by examining the width of the particle stream in the superimposed image. At the inlet of the first spiral (see the images in the left column), particles were uniformly distributed by nature and covered the whole channel width except very close to the walls due to particle–wall interactions [11,12,67]. Once they moved into the curved part of the first spiral, particles started experiencing negative dielectrophoresis as explained above and were thus pushed toward the outer wall. The result was seen to be a squeezed particle stream near the outer wall of the first spiral at the channel center (see the images in the middle column). When they entered into the second spiral, particles were still subject to negative dielectrophoresis, but in the opposite direction, due to the switching of inner and outer walls between the two spirals. Eventually, particles moved out of the double-spiral microchannel in a focused stream near the outer wall of the second spiral (see the images in the right column). These observations (movies are available in supporting information) were confirmed by the numerical modeling.

Fig. 4 compares the experimentally observed electrophoretic motions (left column: snapshot images; middle column: superimposed images) and the numerically predicted trajectories (right column) of 5 μm particles at the outlet of the spiral microchannel under different electric fields (from 100 to 400 V/cm). The correction factor, c, remained at 0.6 for all fields in the modeling. With

[1] For interpretation of color in Fig. 2, the reader is referred to the web version of this article.

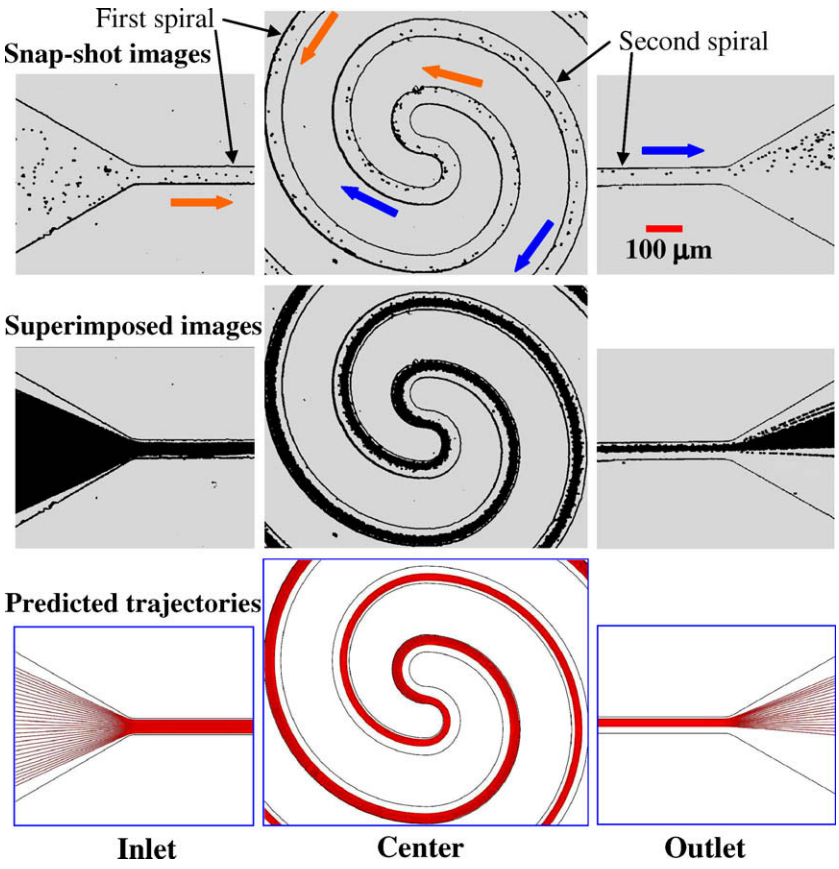

Fig. 3. Illustration and comparison of experimentally observed electrophoretic motions (top row: snap-shot images; middle row: superimposed images) and numerically predicted trajectories (bottom row) of 5 μm particles in the spiral microchannel (left column: inlet; middle column: center; right column: outlet). The applied DC electric field was 200 V/cm on average across the channel length. The block arrows indicate the flow directions.

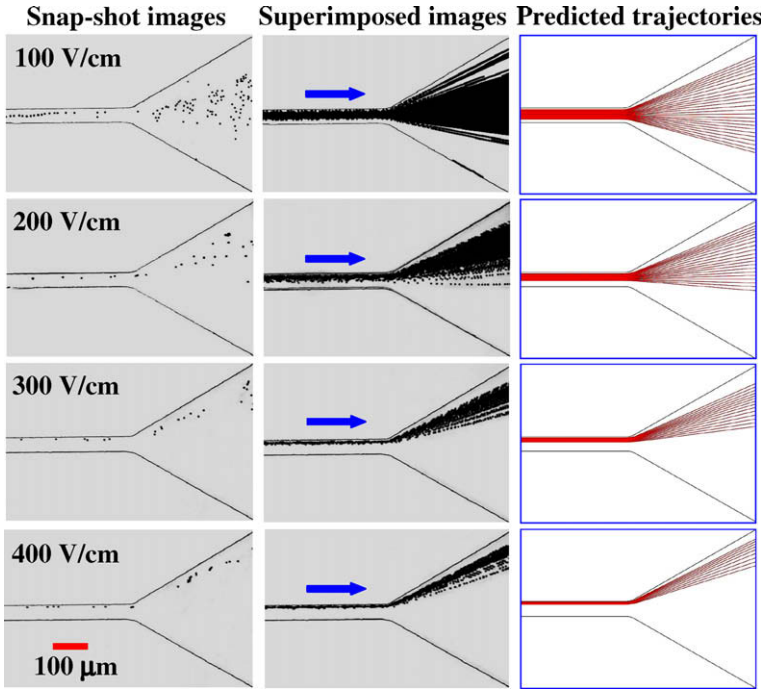

Fig. 4. Comparison of experimentally observed electrophoretic motions (left column: snapshot images; middle column: superimposed images) and numerically predicted trajectories (right column) of 5 μm particles at the outlet of the spiral microchannel at different electric fields (as indicated). The block arrows indicate the flow directions.

the increase of the electric field, particles were focused to a tighter stream, which was also observed to move nearer to the outer wall of the channel (movies are available in the supporting information). Especially at an electric field of 400 V/cm, we noticed that

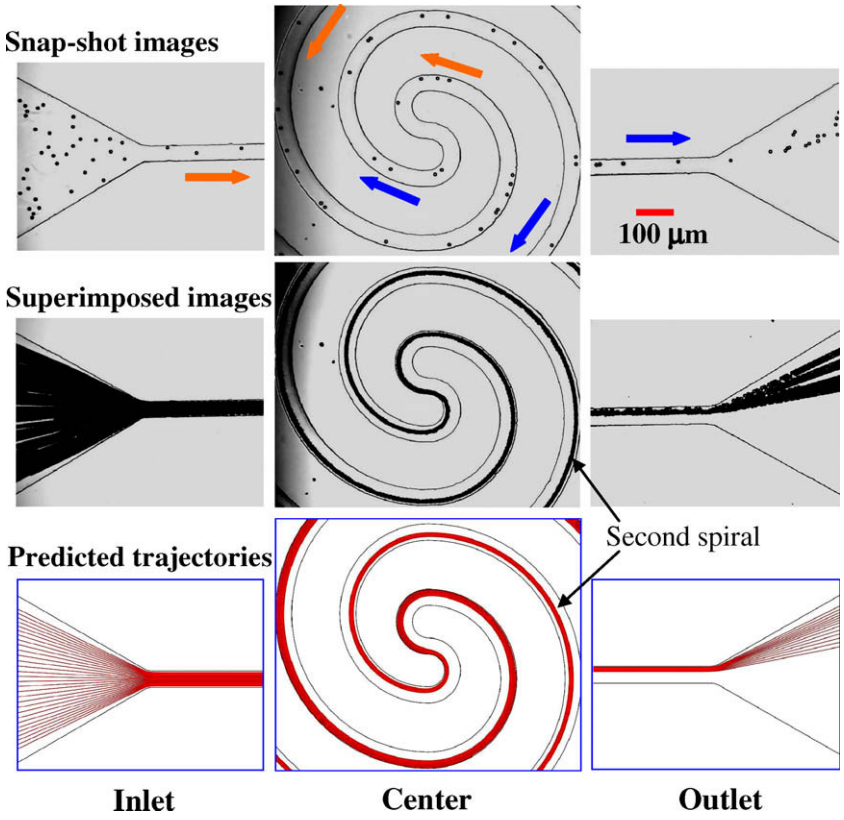

Fig. 5. Illustration and comparison of experimentally observed electrophoretic motions (top row: snap shot images; middle row: superimposed images) and numerically predicted trajectories (bottom row) of 10 μm particles in the spiral microchannel (left column: inlet; middle column: center; right column: outlet). The applied DC electric field was 200 V/cm on average across the channel length. The block arrows indicate the flow directions.

particles were nearly moving in a single file (see the images in the bottom row). This function is expected to find applications in microfluidic flow cytometry [69], particle separation [70], etc. The experimental observations are consistent with the theoretical analysis, as the particle velocity ratio in Eq. (4) does indicate that the curvature-induced dielectrophoretic focusing effects should increase with the increase of the electric field. Moreover, these observations are in reasonable agreement with the numerical simulations, despite the fact that the same correction factor was used in the modeling.

As alluded to earlier, the particle velocity ratio in Eq. (4) also becomes greater for larger particles. This analysis is supported by Fig. 5, which shows the experimentally observed electrophoretic motions (top row: snapshot images; middle row: superimposed images) and the numerically predicted trajectories (bottom row) of 10 μm particles in the spiral microchannel at an electric field of 200 V/cm. The correction factor, c, was set to 0.3 by fitting the width of the focused particle stream in the images at the channel outlet to that predicted in the modeling (see the right column). As compared to the electrophoretic behaviors of 5 μm particles in Fig. 4, we notice that 10 μm particles clearly exhibit larger deflection and better focusing due to stronger curvature-induced dielectrophoresis in the two spirals. These enhanced effects are also apparent in the predicted particle trajectories at the channel center, which, however, seem to be underestimated in the modeling if one compares the position of the focused particle stream in the second spiral of the channel (see the middle column). We attempted to increase the correction factor in the modeling, but still could not get a satisfactory agreement with the experimental data. This discrepancy may be partially attributed to the neglect of particle–wall interactions [11,12,41,68] in our model.

6. Conclusions

We have studied particle electrophoresis in a spiral microchannel using a combined experimental and numerical method. Due to the variation in path length for electric currents, electric field gradients are formed by channel curvatures. As such, particle dielectrophoresis is induced in curved microchannels, and was found to deflect particles across streamlines. The result is a focused particle stream flowing near the outer wall of the spiral channel. Moreover, the width and position of the particle stream at the channel outlet were found to depend on the electric field magnitude and the particle size as predicted from the theoretical analysis. In addition, a numerical model was developed, which simulates closely the observed particle electrophoretic behaviors in the spiral channel in most cases. It is anticipated that the curvature-induced dielectrophoretic focusing effect will find applications in continuous bioparticle separation and flow cytometry for a wide range of technological solutions in biology, medicine, and industry.

Acknowledgments

This work was supported by NSF Grant CBET-0853873 with Marc S. Ingber as the grant monitor.

Appendix A. Supplementary material

Movies of particle electrophoresis at the inlet, center and outlet of the spiral microchannel at different DC electric fields. Supplementary data associated with this article can be found, in the online version, at doi:10.1016/j.jcis.2009.08.031.

References

[1] J. Viovy, Rev. Modern Phys. 7 (2000) 813–872.
[2] O.D. Velev, K.H. Bhatt, Soft Matter 2 (2006) 738–750.
[3] J. Voldman, Annu. Rev. Biomed. Eng. 8 (2006) 425–454.
[4] Y. Kang, D. Li, Microfluid. Nanofluid. 6 (2009) 431–460.
[5] D.C. Henry, Proc. R. Soc. London Ser A 133 (1931) 106–129.
[6] F.A. Morrison, J. Colloid Interface Sci. 34 (1970) 210–214.
[7] R.J. Hunter, Zeta Potential in Colloid Science, Academic Press, New York, 1981.
[8] J. Happel, H. Brenner, Low Reynolds Number Hydrodynamics, Noordhoff International Publishing, Leyden, Netherlands, 1973.
[9] T.B. Jones, Electromechanics of Particles, Cambridge University Press, New York City, NY, 1995.
[10] H.A. Pohl, Dielectrophoresis, Cambridge University Press, Cambridge, 1978.
[11] E. Yariv, Phys. Fluids 18 (2006) 031702.
[12] E. Young, D. Li, Langmuir 21 (2005) 12037–12046.
[13] E.B. Cummings, A.K. Singh, Anal. Chem. 75 (2003) 4724–4731.
[14] B.G. Hawkins, A.E. Smith, Y.A. Syed, B.J. Kirby, Anal. Chem. 79 (2007) 7291–7300.
[15] H.J. Keh, S.B. Chen, J. Fluid Mech. 194 (1988) 377–390.
[16] Y.P. Tang, M.H. Chih, E. Lee, J.P. Hsu, J. Colloid Interface Sci. 242 (2001) 121–126.
[17] E. Yariv, H. Brenner, J. Fluid Mech. 484 (2003) 85–111.
[18] H.J. Keh, J.L. Anderson, J. Fluid Mech. 153 (1985) 417–439.
[19] H.J. Keh, J.Y. Chiou, AICHE J. 42 (1996) 1397–1406.
[20] C. Ye, D. Sinton, D. Erickson, D. Li, Langmuir 18 (2002) 9095–9101.
[21] E. Yariv, H. Brenner, SIAM J. Appl. Math. 64 (2003) 423–441.
[22] H. Liu, H.H. Bau, H.H. Hu, Langmui 20 (2004) 2628–2639.
[23] S.M. Davison, K.V. Sharp, J. Colloid Interface Sci. 303 (2006) 288–297.
[24] S.M. Davison, K.V. Sharp, Nanoscale Microscale Thermophys. Eng. 11 (2007) 71–83.
[25] H. Liu, S.Z. Qian, H.H. Bau, Biophys. J. 92 (2007) 1164–1177.
[26] J.P. Hsu, Z.S. Chen, Langmuir 23 (2007) 6198–6204.
[27] J. Ennis, H. Zhang, G. Stevens, J. Perera, P. Scales, S. Carnie, J. Membrane Sci. 119 (1996) 47–58.
[28] X. Xuan, S. Raghibizadeh, D. Li, J. Colloid Interface Sci. 296 (2006) 743–748.
[29] J. Ennis, J.L. Anderson, J. Colloid Interface Sci. 185 (1997) 497–514.
[30] A. Shugai, S.L. Carnie, J. Colloid Interface Sci. 213 (1999) 298–315.
[31] M.H. Chih, E. Lee, J.P. Hsu, J. Colloid Interfcae Sci. 248 (2002) 383–388.
[32] X. Xuan, C. Ye, D. Li, J. Colloid Interface Sci. 289 (2005) 286–290.
[33] E. Yariv, H. Brenner, Phys. Fluids 14 (2002) 3354–3357.
[34] C. Ye, X. Xuan, D. Li, Microfluid. Nanofluid. 1 (2005) 234–241.
[35] E. Yariv, K.D. Dorfman, Phys. Fluids 19 (2007) 037101.
[36] K.D. Dorfman, Phys. Fluids 20 (2008) 037102.
[37] X. Xuan, B. Xu, D. Li, Anal. Chem. 77 (2005) 4323–4328.
[38] S.Z. Qian, A.H. Wang, J.K. Afonien, J. Colloid Interface Sci. 303 (2006) 579–592.
[39] Y. Ai, S. Joo, Y. Jiang, X. Xuan, S. Qian, Electrophoresis 30 (2009) 2399–2506.
[40] I. Barbulovic-Nad, X. Xuan, J. Lee, D. Li, Lab Chip 6 (2006) 274–279.
[41] K. Kang, X. Xuan, Y. Kang, D. Li, J. Appl. Phys. 99 (2006) 064702.
[42] J. Zhu, X. Xuan, Electrophoresis 30 (2009) 2668–2675.
[43] M.D. Pysher, M.A. Hayes, Anal. Chem. 79 (2007) 4552–4557.
[44] S.K. Griffiths, R.H. Nilson, Anal. Chem. 72 (2000) 5473–5482.
[45] J.I. Molho, A.E. Herr, B.P. Mosier, J.G. Santiago, T.W. Kenny, R.A. Brennen, G.B. Bordon, B. Mohammadi, Anal. Chem. 73 (2001) 1350–1360.
[46] S.M. Davison, K.V. Sharp, Microfluid. Nanofluid. 4 (2008) 409–418.
[47] C. Ye, D. Li, J. Colloid Interface Sci. 272 (2004) 480–488.
[48] X. Xuan, D. Li, Electrophoresis 26 (2005) 3552–3560.
[49] J. Zhu, T.J. Tzeng, G. Hu, X. Xuan, Microfluid. Nanofluid. 7 (in press), doi: 10.1007/s10404-009-0432-7.
[50] M. Zourob, S. Mohr, A.G. Mayes, A. Macaskill, N. Perez-Moral, P.R. Fielden, N.J. Goddard, Lab Chip 6 (2006) 296–301.
[51] A.P. Sudarsan, V.M. Ugaz, Lab Chip 6 (2006) 74–82.
[52] D. Di Carlo, D. Irimia, R.G. Tompkins, M. Toner, Proc. Natl. Acad. Sci. 104 (2007) 18892–18897.
[53] J. Seo, M.H. Lean, A. Kole, Appl. Phys. Lett. 91 (2007) 033901.
[54] J. Seo, M.H. Lean, A. Kole, J. Chromatogr. A 1162 (2007) 126–131.
[55] D. Di Carlo, J.F. Edd, D. Irimia, R.G. Tompkins, M. Toner, Anal. Chem. 80 (2008) 2204–2211.
[56] A.A.S. Bhagat, S.S. Kuntaegowdanahalli, I. Papautsky, Lab Chip 8 (2008) 1906–1914.
[57] D.H. Yoon, J.B. Ha, Y.K. Bahk, T. Arakawa, S. Shojib, J.S. Go, Lab Chip 9 (2009) 87–90.
[58] D. Li, Electrokinetics in Microfluidics, Elsevier, Academic Press, 2004.
[59] L.G. Leal, Annu. Rev. Fluids Mech. 12 (1980) 435–476.
[60] S.A. Berger, L. Talbot, L. Yao, Annu. Rev. Fluids Mech. 15 (1983) 461–512.
[61] H. Morgan, N.G. Green, AC Electrokinetic: Colloids and Nanoparticles, Research Studies Press, Berlin, 2002.
[62] I. Ermolina, H. Morgan, J. Colloid Interface Sci. 285 (2005) 419–428.
[63] E.B. Cummings, S.K. Griffiths, R.H. Nilson, P.H. Paul, Anal. Chem. 72 (2000) 2526–2532.
[64] J.L. Anderson, Annu. Rev. Fluids Mech. 21 (1989) 61–99.
[65] D.C. Duffy, J.C. McDonald, O.J.A. Schueller, G.M. Whitesides, Anal. Chem. 70 (1998) 4974–4984.
[66] K. Kang, Y. Kang, X. Xuan, D. Li, Electrophoresis 27 (2006) 694–702.
[67] W.B. Russel, D.A. Saville, W.R. Schowalter, Colloidal Dispersions, Cambridge University Press, 1992.
[68] K. Kang, D. Li, Langmuir 22 (2006) 1602–1608.
[69] D.A. Ateya, J.S. Erickson, Jr.P.B. Howell, L.R. Hilliard, J.P. Golden, F.S. Ligler, Anal. Bioanal. Chem. 391 (2008) 1485–1498.
[70] N. Pamme, Lab Chip 7 (2007) 1644–1659.